JGR Atmospheres

RESEARCH ARTICLE
10.1029/2020JD033103

Differences Between ICESat and CryoSat-2 Sea Ice Thicknesses Over the Arctic: Consequences for Analyzing the Ice Volume Trend

Jong-Min Kim[1,2], Byung-Ju Sohn[1,3], Sang-Moo Lee[1,4,5], Rasmus Tage Tonboe[6], Eui-Jong Kang[1], and Hyun-Cheol Kim[2]

[1]School of Earth and Environmental Sciences, Seoul National University, Seoul, South Korea, [2]Unit of Arctic Sea-Ice Prediction, Korea Polar Research Institute, Incheon, South Korea, [3]Key Laboratory for Aerosol-Cloud-Precipitation of China Meteorological Administration, School of Atmospheric Physics, Nanjing University of Information Science and Technology, Nanjing, China, [4]Department of Electrical, Computer, and Energy Engineering, Center for Environmental Technology, University of Colorado, Boulder, CO, USA, [5]National Snow and Ice Data Center, University of Colorado, Boulder, CO, USA, [6]Danish Meteorological Institute, Copenhagen, Denmark

Abstract Two sources of readily available and non-overlapping space-borne data on sea ice thickness over the Arctic (i.e., Ice, Cloud, and land Elevation Satellite [ICESat] and CryoSat-2 [CS2]) were compared using overlapping thermal microwave radiometer data to examine their respective differences. As a bridge connecting these two data sets, data on the vertically polarized emissivity difference between 10.65 and 18.7 GHz derived from the Advanced Microwave Sounding Radiometer were related to ICESat and CS2 thickness values via regression. The results indicate that there are substantial and systematic differences in the ice thickness between these two data sets over the Arctic; ICESat ice thickness was systematically lower than that of CS2 by ~50 cm, compared to ice thickness from Operation IceBridge and upper looking sonar data. The CS2 thickness observed later than that of ICESat was found to be thicker, contradicting the thinning expected under global warming conditions. Correcting for the 50-cm difference between ICESat or CS2 data revealed trends in ice volume that are consistent with the expected and modeled declines in the Pan-Arctic Ice-Ocean Modeling and Assimilation System data, further corroborating the 50 cm of relative bias observed between the two data sets.

Key Points:
- The ICESat and Cryosat-2 ice thickness data sets, which have a 24-month gap, were compared
- A systematic and substantial difference of ~50 cm was found between the ICESat and CryoSat-2 data sets
- Snow depth used for estimating the ice thickness is found to be one of major sources of uncertainty causing the difference

Supporting Information:
- Supporting Information S1

Correspondence to:
B.-J. Sohn,
sohn@snu.ac.kr

Citation:
Kim, J.-M., Sohn, B.-J., Lee, S.-M., Tonboe, R. T., Kang, E.-J., & Kim, H.-C. (2020). Differences between ICESat and CryoSat-2 sea ice thicknesses over the Arctic: Consequences for analyzing the ice volume trend. *Journal of Geophysical Research: Atmospheres*, *125*, e2020JD033103. https://doi.org/10.1029/2020JD033103

Received 14 MAY 2020
Accepted 28 OCT 2020
Accepted article online 3 NOV 2020

©2020. The Authors.
This is an open access article under the terms of the Creative Commons Attribution License, which permits use, distribution and reproduction in any medium, provided the original work is properly cited.

1. Introduction

The extent and volume of sea ice are important parameters for understanding and projecting the evolution of Arctic sea ice, especially in the context of ongoing anthropogenic warming. Their importance owes to the fact that sea ice extent has a substantial influence on the surface energy balance of the Arctic Ocean (Comiso et al., 2003; Maykut, 1978; Maykut & Untersteiner, 1971), while the variation of sea ice extent directly affects changes in ice volume (i.e., extent multiplied by thickness of sea ice). Thus, accurate measurements of the extent and thickness of sea ice are critical for better modeling and projection of sea ice dynamics.

Sea ice extent is commonly estimated from space-borne microwave measurements, which have the advantages of providing all-sky measurements (i.e., during both day and night and under clear and cloudy conditions) and the availability of long-term measurements beginning in 1978 (Cavalieri et al., 1984; Comiso, 1995; Lavergne et al., 2019; Markus & Cavalieri, 2000; Spreen et al., 2008; Tonboe et al., 2016). Although there remain problems in estimating ice concentration of new ice or during the summer melting season, the level of uncertainty for the total ice extent over the Arctic is claimed to be ~1%, even for the summer (Meier & Stewart, 2019). Using the available, long-term, microwave-based sea ice extent data, it is now possible to assess future projections of Arctic sea ice, as exemplified by Peng et al. (2018), who reported that the Arctic Ocean may be nearly ice-free in summer by the year 2037.

In contrast to ice extent, measuring ice thickness from space is challenging because altimeters measure the sea ice freeboard or the total freeboard, which are then converted into ice thickness (Laxon et al., 2013; Zwally et al., 2002). Furthermore, the poor spatial and temporal coverage of satellite-derived sea ice thickness also remains challenging when compared to other data sets. The Ice, Cloud, and land Elevation

Satellite (ICESat) was launched in January of 2003, carrying a lidar altimeter for measuring the total freeboard (Kwok & Cunningham, 2008; Zwally et al., 2002). Ice thickness retrieval from ICESat was stopped in October 2008, although the mission continued until October 2009. It may be due to less reliable freeboard measurements when the ICESat mission approached the end phase. CryoSat-2 (CS2) was launched on 8 April 2010, with preliminary science observations being received at the conclusion of the Launch and Early Orbit Phase, a few days later. It carries a radar altimeter to measure the sea ice freeboard (Laxon et al., 2013). The two ice thickness retrieval algorithms employed by these satellites have different sensitivities to inputs of snow depth (Zygmuntowska et al., 2014) and different sensor technologies. Furthermore, the 24-month gap from the loss of high-quality ICESat returns to the beginning of the CS2 operational mission (i.e., November of 2008 to November of 2010), hindering the data production of a continuous record of ice thickness, as well as the direct comparison of the products of these two satellites (WMO, 2020; Yi & Zwally, 2009). Nevertheless, after combining the two sets of ice thickness data with sea ice extent data, a dramatic loss in ice volume over the Central Arctic was documented (Kwok & Cunningham, 2015; Laxon et al., 2013). However, there is a concern that the observed change in volume from the two data sets may be prone to substantial uncertainties, largely due to different inputs, such as the snow depth and snow/ice density for converting the estimated freeboard into ice thickness (Zygmuntowska et al., 2014).

Effective combination of ICESat and CS2 data to investigate any trends linked to ice thickness requires homogenization of the two data sets to bridge the aforementioned 24-month gap in their data available periods. In this study, it is examined whether the two data sets meet the requirements for using them as a combined data set. In doing so, it is also investigated whether there were any respective differences between the two data sets that may influence their trends. First, a common index is developed from Advanced Microwave Scanning Radiometer (AMSR) brightness temperatures, which can be used as a common platform for comparing ICESat and CS2 sea ice thicknesses. The results will provide an estimate of how the two sets of ice thickness data may differ from each other so that the trends in sea ice thickness (or volume) could be estimated with a likelihood of offsets.

2. Used Data

2.1. ICESat Ice Thickness

The ICESat, which was launched in January of 2003, measured the snow surface height from water level (i.e., total freeboard) using the 1,064-nm Geoscience Laser Altimeter System (GLAS) for 2003–2008 (Kwok & Cunningham, 2008; Yi et al., 2011). The total freeboard was then converted to ice thickness based on the assumption that the snow and sea ice over the ocean were in the hydrostatic balance. In this estimation procedure, both snow depth and the densities of seawater, sea ice, and snow must be prescribed. At the National Snow and Ice Data Center (NSIDC), where the ICESat data were obtained for this study—actual data were produced at the National Aeronautics and Space Administration (NASA) Goddard Space Flight Center (GSFC) Science Investigator-led Processing System (SIPS)—the snow climatology of Warren et al. (1999) was used as the snow depth input (Yi & Zwally, 2009).

The ICESat observed the total freeboard for approximately 3 months each year, mainly the periods from February to March (FM), May to June (MJ), and October to November (ON), within operational campaigns that extended the lifespan of its instruments (Schutz et al., 2005), and the temporal coverage varied each year (http://nsidc.org/data/NSIDC-0393). In this study, observations were used only from March of 2004–2008. The details regarding ICESat data are available on the NSIDC website (http://nsidc.org/data/NSIDC-0393; Yi & Zwally, 2009). The temporal coverages of major data sets used in this study are summarized in Figure 1, and their spatial and temporal resolutions are provided in Table 1.

2.2. CS2 Ice Thickness

In contrast to ICESat measurements of the total freeboard (including snow cover), CS2 measures the ice height above the water level (i.e., sea ice freeboard) using a microwave, 13.575-GHz, Ku-band radar altimeter (Laxon et al., 2013; Wingham et al., 2006). The measured freeboard of the sea ice is then converted to sea ice thickness with prescribed snow depth and densities of snow and ice to solve the presumed hydrostatic balance equation. Similar to the ice thickness retrieval from ICESat measurements, snow depth has been recognized as an input parameter that causes the greatest uncertainty during ice thickness retrieval (Kwok &

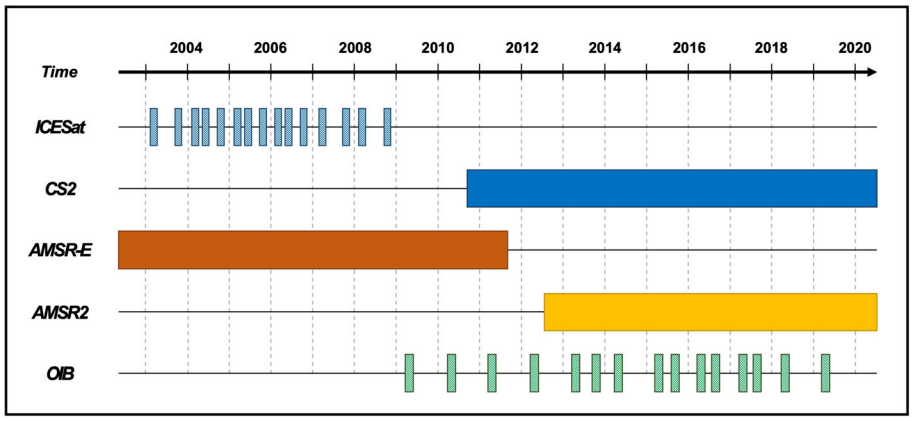

Figure 1. Temporal spans of various data sets used in this study. Full expressions of the abbreviated data names are found in the text. Intermittent bars for ICESat and OIB represent the intermittent periods of available data.

Cunningham, 2008). In the CS2 data processing at the NSIDC, the same snow climatology of Warren et al. (1999) was used as input to solve the hydrostatic balance equation for ice thickness.

The CS2 is still operational, with an extended, continuous observation period of over 10 years. The temporal coverage is also continuous throughout the year, unlike the intermittent observations of ICESat. The CS2 level-4 ice thickness data, based on the method of Kurtz et al. (2014), were obtained from the NSIDC (https://nsidc.org/data/RDEFT4/; Kurtz & Harbeck, 2017), but only March data were used in this analysis in order to match the ICESat data.

2.3. AMSR Brightness Temperature Data

The AMSR-E mission, which measured the passive microwave brightness temperatures at 6.925, 10.65, 18.7, 23.8, 36.5, and 89.0 GHz, operated from May of 2002 until October of 2011 (Imaoka et al., 2012). The subsequent AMSR2 mission began measuring brightness temperatures at the same frequencies as in AMSR-E in June of 2012, leaving a 9-month gap between the two missions. In this study, AMSR-derived vertically polarized emissivity differences (EVDs) were regressed to either the ICESat or CS2 ice thickness (see section 3 for the discussion of the EVD). To derive the EVDs, brightness temperatures at 6.925, 10.65, and 18.7 GHz, as measured in the AMSR-E and AMSR2 missions, were then used for the period 2004–2018. Gridded, level-3 data at a spatial resolution of 25 × 25 km were obtained from the Global Change Observation Mission (GCOM) website (https://gportal.jaxa.jp/).

2.4. Ice Concentration and Age Products

To derive the EVDs from AMSR-E/AMSR2-measured brightness temperatures, it was necessary to first decide whether or not the target was covered with ice. The March mean ice concentration data from 2004–2018, based on the bootstrap algorithm presented by Comiso et al. (2003), were downloaded from the same GCOM website (https://gportal.jaxa.jp/). Ice concentration data were also used for determining the ice area, which was used to calculate the total ice volume. Additionally, Equally Area Scalable Earth grid (EASE-grid) sea ice age data (version 4; https://nsidc.org/data/nsidc-0611/; Tschudi et al., 2019) from the NSIDC were used to separate first-year from multiyear sea ice. Using information on sea ice age, the first-year sea ice was separated from the multiyear ice so that microwave-based EVDs could be related to the altimeter-based sea ice thickness for the first-year or multiyear ice separately. During NSIDC ice age data processing, the ice age was determined by tracking moving ice targets and adding 1 year to the last year's age if the target survived the summer (Tschudi et al., 2019). Monthly ice age data were constructed from the original weekly data and placed in an AMSR 25 × 25 km spatial grid format. As for the ice concentration, mean ice age data from March of 2004–2018 were used for regression analysis.

2.5. OIB Data

In order to assess the possible systematic differences between ICESat and CS2 ice thickness data, the AMSR EVD-estimated ice thicknesses were compared with the common ice thickness data from Operation IceBridge (OIB), whose missions were arranged to bridge the gap between ICESat-1 and

Table 1
Periods of ICESat, CS2, AMSR-E, AMSR2, and OIB Data Used for Obtaining Regression Equations and for Assessing the Difference

		Used data period
Regression	ICESat	1–21 March 2004 1–24 March 2005 1–28 March 2006 12–31 March 2007 1–21 March 2008
	CS2	1–31 March 2011, 1–31 March of 2013–2018
	AMSR-E	1–31 March of 2004–2008, 1–31 March 2011
	AMSR2	1–31 March of 2013–2018
Validation	AMSR-E vs. OIB	31 March and 2, 5, 21, and 25 April 2009 23 and 26 March and 2, 5, 12, 19, 20, and 21 April 2010

ICESat-2 (Farrell et al., 2011), the latter of which was launched in September of 2018. The OIB is an airborne campaign for measuring various snow- and ice-related parameters over the Arctic. In this study, we used the snow top height relative to the sea surface, employing a 532-nm Airborne Topographic Mapper (ATM), and the snow depth determined from a combination of ATM and snow radar measurements (Kurtz et al., 2013). In other words, the directly measured snow depth was used as input for solving the hydrostatic balance equation to obtain the sea ice thickness from the ATM-measured total freeboard.

As an airborne campaign, the spatial coverage of OIB is restricted along flight paths, which are mainly over the Central Arctic Ocean, Beaufort Sea, and northern coast of Greenland. The temporal coverage of OIB is intermittent. The OIB data collected during March–April of 2009 and 2010, when there was a gap between ICESat and CS2 data, were used to assess the presumed differences in ice thickness between the ICESat and CS2 data sets. In this study, the OIB version-1, Level-4 sea ice thickness data were obtained at a spatial resolution of 40 m from the NSIDC IceBridge website (http://nsidc.org/data/idcsi4/). The observation dates available during the target period are summarized in Table 2.

2.6. PIOMAS Ice Thickness

We examine how the possible differences between ICESat and CS2 ice thickness data may cause differences in their respective ice volume trends. In doing so, obtained results were compared against the volume trends estimated from Pan-Arctic Ice-Ocean Modeling and Assimilation System (PIOMAS) ice thickness. The PIOMAS is a numerical model with sea ice and ocean components and the capacity for assimilating various observations; it has been extensively validated with various in situ observations from submarines, moorings, and aircrafts (Schweiger et al., 2011; Stroeve et al., 2015). The uncertainties of the PIOMAS ice thickness are reported to range from −0.01 to −0.17 m for the mean bias and from 0.68 to 0.78 m for the root mean square deviation (RMSD), leading to a rather small volumetric uncertainty of 0.1×10^3 km^3 for March. Here, March mean ice thickness data for 2004–2018 are used, in order to examine trends in ice volume. The PIOMAS data were downloaded from the Polar Science Center (PSC) website (http://psc.apl.uw.edu/).

3. Theoretical Background and Analysis Procedure

3.1. Optical Properties of Sea Ice Varying With Ice Thickness

As shown in Figure 1, there is a temporal gap between the ICESat and CS2 ice thickness data, which prohibited direct comparison between the two data sets. However, because the microwave measurements from the AMSR-E mission cover this gap, we attempt to bridge the two data sets by using the AMSR-E as a common platform. To achieve such bridging, first, a microwave-based index is developed for linking to the altimeter-based ice thickness.

In the Arctic, when the saline first-year ice is formed, the lower-frequency microwave signal emitted from the ice layer just beneath the snow-ice interface can transfer to the snow surface without much scattering or absorption in the snow and ice, as shown in Figure 2a. This is because the scattering of radiation by the brine in the sea ice or by snow grain structures is less effective at lower microwave frequencies. In contrast, for the multiyear sea ice, which has survived the summer melting season, the brine in the first-year sea

Table 2
Spatial and Temporal Resolutions of Used Data Sets Listed in Table 1

	Product name	Spatial resolution	Temporal resolution
Regression	JAXA AMSR-E/AMSR2 L3 Daily Brightness Temperature	25 km	Daily
	NSIDC Arctic Sea Ice Freeboard and Thickness, Version 1	170 m	Irregular
	NSIDC CryoSat-2 Level-4 Sea Ice Elevation, Freeboard, and Thickness, Version 1	25 km	Monthly
Validation	JAXA AMSR-E/AMSR2 L3 Daily Brightness Temperature	25 km	Daily
	NSIDC IceBridge L4 Sea Ice Freeboard, Snow Depth, and Thickness, Version 1	40 m	Occasional

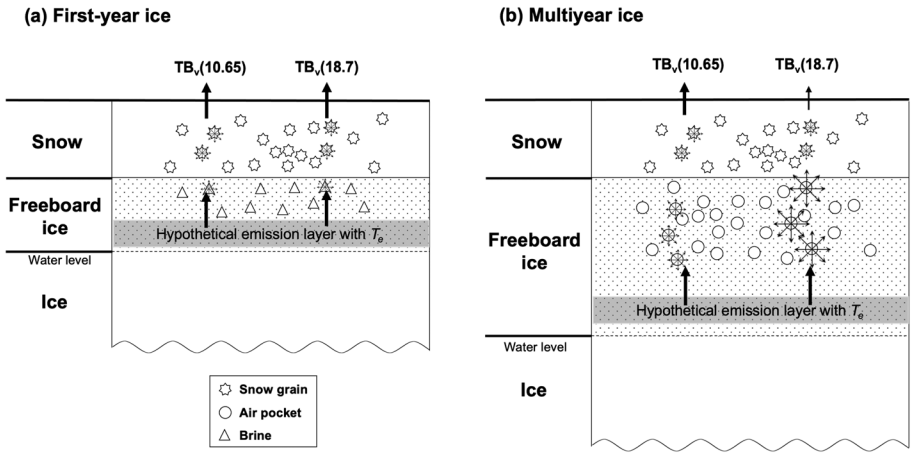

Figure 2. Schematic diagrams of the hypothetical emitting layer and microwave radiative transfer within snow and ice layer for (a) the first-year ice and (b) the multiyear sea ice. Nomenclatures and detailed explanations are found in the text. The arrow size represents the relative magnitude of emitted or transferred microwave radiation. In (b), the shorter arrows at the snow top express reduced radiation by the scattering and the narrower arrow at 18.7 GHz represents a relatively larger scattering effect for higher 18.7 GHz frequency, compared with 10.65 GHz.

ice will be drained out and replaced by scatterers in the freeboard sea ice (Comiso, 1983; Cox & Weeks, 1974). The loose structure and reduced salinity of the freeboard ice in multiyear ice allows the radiation to penetrate deeper, and thus, the microwave emitting layer of the multiyear ice is also deeper. Since air pockets scatter radiation, the radiation emitted from the deeper layer is more affected by such air pockets (Comiso, 1983; Hewison & English, 1999), when compared to first-year sea ice (Figure 2b). Thus, the degree to which the emitted radiation is scattered is linked to the ice thickness because the freeboard sea ice thickness is proportional to the ice thickness, and thicker multiyear ice scatters more than first-year ice. Furthermore, more scattering can be expected at higher frequencies (here, 18.7 GHz) for multiyear ice.

The changes in optical properties between the first-year and multiyear sea ice, and from lower freeboard to higher freeboard, suggest that there may be a way to estimate the sea ice thickness, at least for the multiyear sea ice, from passive microwave measurements. In order to examine the possibility of inferring sea ice thickness from such measurements, the vertically polarized surface emissivity at 10.65 and 18.7 GHz is defined, by assuming the 6.9 GHz-derived sea ice interface temperature (Lee et al., 2017) to be the temperature of the emission layer (Equations 1 and 2).

$$\varepsilon_V(10.65) = \frac{TB_v(10.65)}{T_e(6.9)} \tag{1}$$

$$\varepsilon_V(18.7) = \frac{TB_v(18.7)}{T_e(6.9)}, \tag{2}$$

where TB_v and T_e are the vertically polarized brightness temperature at the surface and the emission layer temperature, respectively, and the number in parenthesis represents the microwave frequency in gigahertz. These definitions are shown schematically in Figure 2.

Emissivity differences between the first-year and multiyear sea ice should be evident at either 10.65 or 18.7 GHz due to scattering in the multiyear sea ice, although the threshold separating the first-year ice from the multiyear ice should be difficult to determine when a one-channel approach is used. However, the emissivity difference between two channels carries a different scattering layer signal from the freeboard sea ice. The two-channel emissivity difference for the first-year sea ice may be small (near zero) because of the limited influence of scattering on first-year freeboard ice. In contrast, the emissivity difference between two channels for the multiyear sea ice may vary proportionally with sea ice thickness, wherein thicker sea ice means thicker freeboard ice, which can cause greater scattering at higher frequencies (Lee et al., 2018; Mathew et al., 2009).

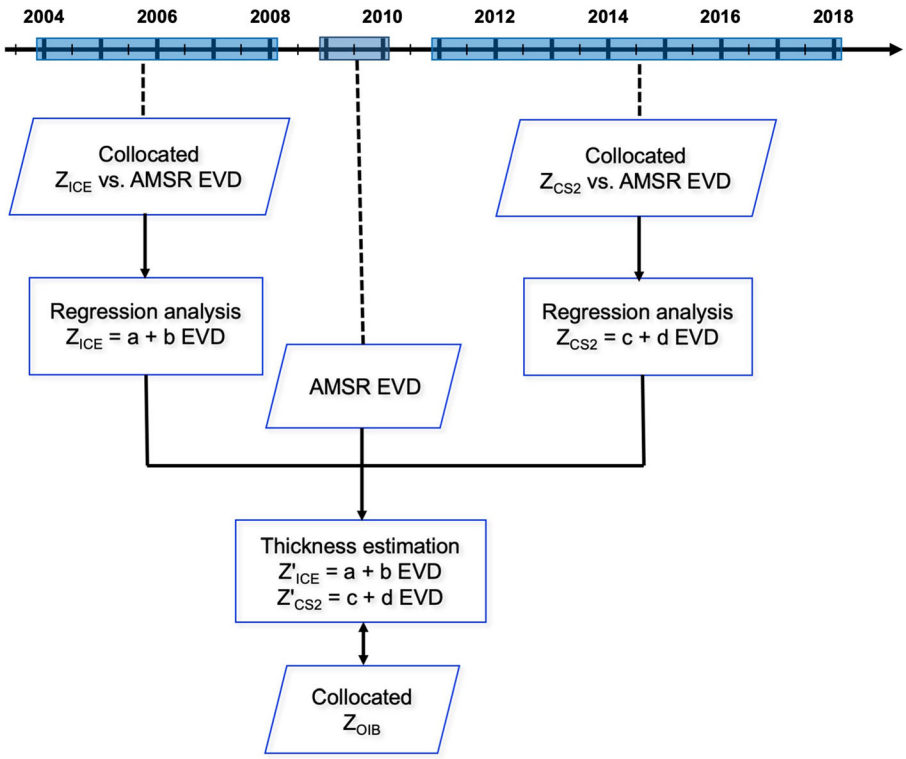

Figure 3. Schematic diagram showing the analysis procedures used in this study.

To reflect the physical reasoning of the emissivity differences between two channels, the EVD is introduced as an index representing sea ice thickness, such that

$$EVD = \varepsilon_V(10.65\,\mathrm{GHz}) - \varepsilon_V(18.7\,\mathrm{GHz}). \quad (3)$$

A larger EVD in Equation 3 implies a higher freeboard sea ice and thus thicker sea ice. The EVD index has been successfully used for differentiating between first-year and multiyear sea ice (Lee et al., 2017). The emissivity at each channel in Equation 3 is calculated as a ratio between the emission layer temperature (T_e) and brightness temperature at the surface (TB_v), such that $\varepsilon_v = TB_v/T_e$, as described in Figure 2. The atmospheric correction is also made to obtain the brightness temperature at the surface from the satellite-measured brightness temperature, although its magnitude was found to be insignificant. Errors can be induced by using the 6.9 GHz emission layer temperature for 10.65 and 18.7 GHz emission temperatures because the lower-frequency microwave can penetrate deeper, and thus, all three channels can have different emission layer depths. However, the errors induced by such assumptions were found to be minimal, with error ranges of <1% for both 10.65 and 18.7 GHz (Lee et al., 2017). Furthermore, this error may not be counted as an error when the emissivities in Equations 1 and 2 are defined to represent a ratio to the emission temperature at 6.9 GHz. It is also worth noting that the scattering effects of snow on 10.65 and 18.7 GHz emissivities were also minimal, as shown by the calculated effects being <1% at these frequencies (Lee et al., 2017).

3.2. Analysis Procedure

Once EVDs are calculated from AMSR-measured brightness temperatures, the analysis procedures for examining the possible difference between two data sets are presented in Figure 3. First, the ICESat and CS2 ice thickness are mapped to the corresponding AMSR EVD by separately conducting the linear regression analysis, that is, Z_{ICE} = a + b EVD and Z_{CS2} = c + d EVD expressed in Figure 3. Then, obtained two regression equations are applied to common AMSR EVD data for the 2009–2010 period, where the data gap exists between the ICESat and CS2 ice thickness, to estimate the ICESat-equivalent and CS2-equivalent ice

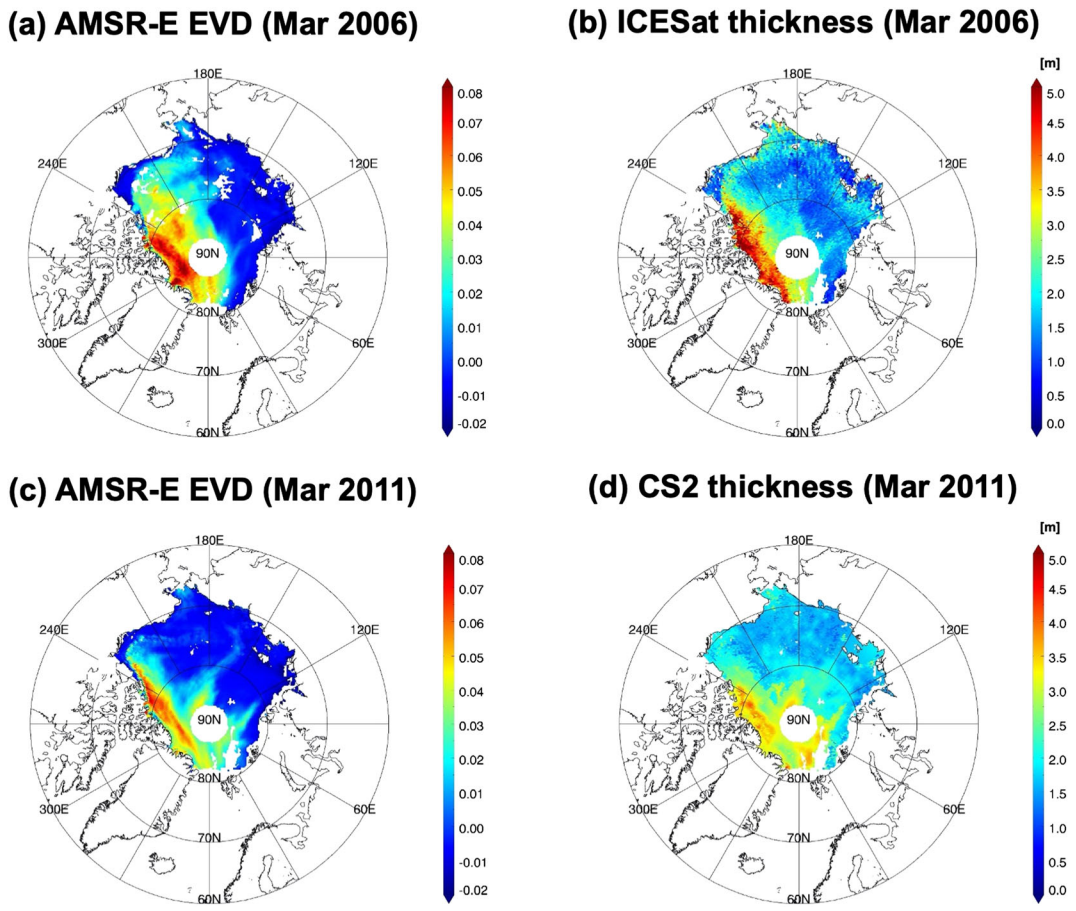

Figure 4. (Left panels) Geographical distributions of EVD on (a) March 2006 and (c) March 2011. (Right panels) Geographical distributions of the sea ice thickness (b) from ICESat and (d) CS2, corresponding to EVD distributions in left panels.

thickness (i.e., Z'_{ICE} and Z'_{CS2} in Figure 3). At this point, those obtained Z'_{ICE} and Z'_{CS2} are compared with the collocated airborne OIB measurements of ice thickness (Z_{OIB}) as a reference, for assessing the relative differences between Z'_{ICE} and Z'_{CS2}.

4. Results

4.1. Development of Ice Thickness Estimation Model and Evaluation

4.1.1. EVD Versus Ice Thickness

To relate the EVD to the altimeter-based ice thickness, daily EVDs were calculated from AMSR-E and AMSR2 brightness temperatures, and then, the EVDs were averaged over a 25 × 25 km equal-area grid to generate a monthly mean of EVD. Monthly mean ice concentration and ice age data were also formatted in the same grid. By collocating the ICESat sea ice thickness with the AMSR-derived EVD, the monthly composite estimate of sea ice thickness was constructed by taking an average of all instantaneous footprints located in each AMSR 25 × 25 km grid over the corresponding month, but only if the total number of data points exceeded 150 (i.e., ~60% of all theoretically available data points). However, the monthly composite was rejected if the monthly mean sea ice concentration of the AMSR grid point was less than 98% or if the AMSR grid point was located within 100 km of the coastline.

In order to examine the quality of the EVD-derived ice thickness, the AMSR-E-derived EVD is compared with the ICESat-estimated ice thickness for March of 2006 and with the CS2 for March of 2011 (Figure 4). This comparison indicates that there is a general agreement between the EVD- and altimeter-derived ice thicknesses over the high EVD area (e.g., EVD > 0.02). However, there is little agreement between the two fields over the area where the EVDs have near-zero values. Considering that those high and near-zero EVD areas

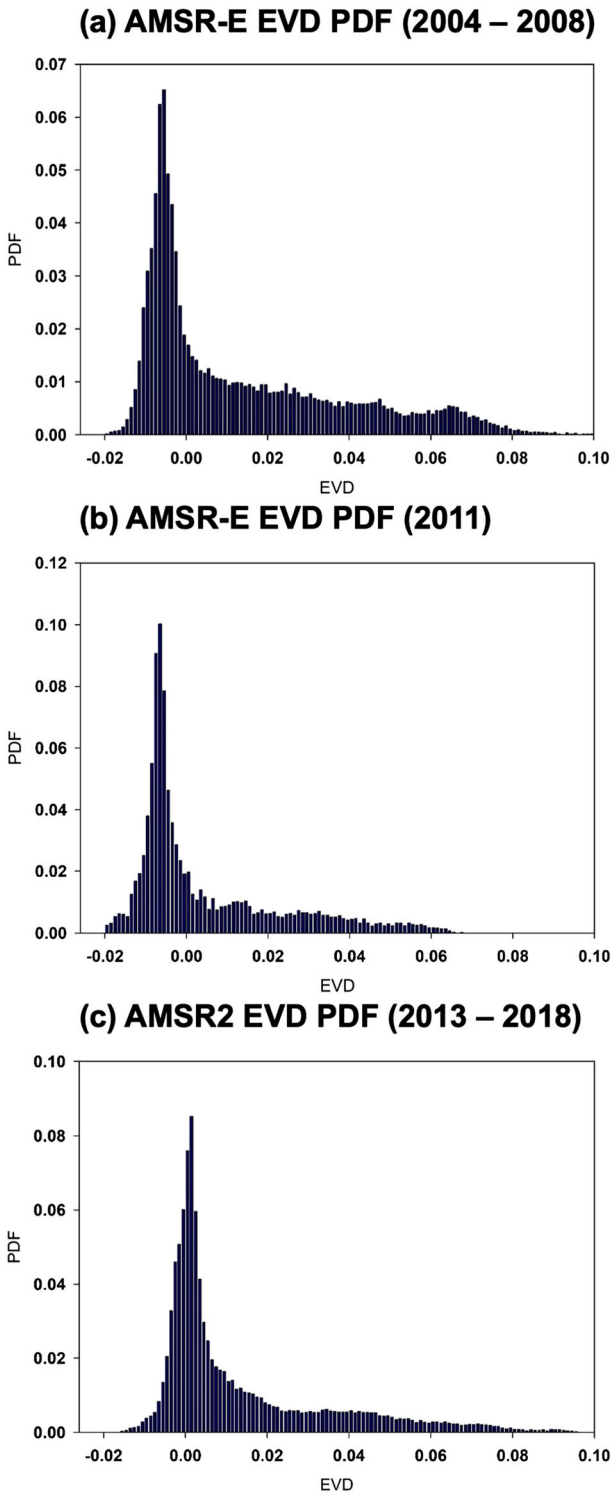

Figure 5. Probability distribution functions of (a) AMSR-E EVD in March of 2004–2008, (b) AMSR-E EVD in March 2011, and (c) AMSR2 EVD in March of 2013–2018.

generally correspond to multiyear and first-year sea ice areas, respectively, the plots suggest that the multiyear sea ice thickness can be estimated by relating the EVD to altimetry-based ice thickness data, but it may not be used over first-year ice. This inapplicability of the EVD method to the first-year ice is expected from the aforementioned optical properties, since emissivity differences may not be discernable among first-year sea ice.

Before examining the relationship between EVD and altimeter-based sea ice thickness, the consistency between AMSR-E and AMSR2 measurements is evaluated, as there is a 9-month gap between the two missions. The distributions of probability density function (PDF) of EVD are plotted for two AMSR-E periods (2004–2008 and 2011) and for an AMSR2 period (2013–2018), assuming that the first-year sea ice should have a common mode near zero EVD (Figure 5). The three periods of plotted PDFs correspond to the periods of AMSR-E EVD versus ICESat ice thickness, AMSR-E EVD versus CS2 ice thickness, and AMSR2 EVD versus CS2 ice thickness, respectively. It is shown that the peak mode appears nearly invariant between ICESat and CS2 when AMSR-E is used (i.e., during the first two periods). However, the EVD peak mode for AMSR2 (i.e., the final period) appears to be slightly larger than that for AMSR-E, even when the same CS2 is used; this is likely due to the different sensor characteristics of the two AMSR missions, including calibration uncertainties. To ensure a consistent EVD, the AMSR2 EVD is adjusted to equalize the peak modes; AMSR2 EVDs were adjusted by subtracting 0.0068 to yield the same first-year sea ice mode shown in Figure 5a (i.e., −0.0056). The subtracted EVD value is found to be caused by the systematic differences in brightness temperatures at three channels between AMSR-E and AMSR2 (JAXA, 2020).

After the EVDs between AMSR-E and AMSR2 are homogenized, AMSR-based EVDs are collocated with the sea ice thickness data from the two satellites, and plots are made separately for the multiyear and first-year sea ice using the corresponding ice age information obtained from the NSIDC ice age data (Figure 6). Here, we separate the multiyear ice from the first-year ice using a 1-year-old criterion of the ice age. It is notable that the plots for the multiyear ice show a linear relationship between the EVD and sea ice thickness, with correlation coefficients of 0.73 for AMSR-E versus ICESat and 0.78 for AMSR-E/AMSR2 versus CS2. The obtained regression equations are $y = 26.89x + 1.34$ for ICESat and $y = 25.55x + 1.88$ for CS2, where x and y are the EVD and ice thickness, respectively. Standard errors of y intercepts are found to be 0.8 cm for ICESat and 0.4 cm for CS2, which are much smaller compared to the intercept difference between two lines, ~50 cm.

The root mean squared errors (RMSEs) associated with ICESat and CS2 regressions were found to be 0.60 and 0.48 m, respectively. Although the RMSE tells us how far the data points are from the regression line, it is difficult to apply the mean RMSE for further analyses, such as the comparison against OIB measurements (Figures 7 and 8) and the calculation of Arctic ice volume trends (Figure 10) because the RMSE appears to be EVD-dependent. Thus, instead of using the mean RMSE, the EVDs are binned with the corresponding error ranges for ICESat and CS2 ice thickness; Figure 6 shows the binned error ranges associated with a standard deviation of ±1 for each bin. The binned error ranges are then kept for estimating errors in subsequent analyses using EVD-derived sea ice thickness. From now on, the error range is referred to as the mean standard deviation of all binned EVD-derived sea ice thickness in Figure 6.

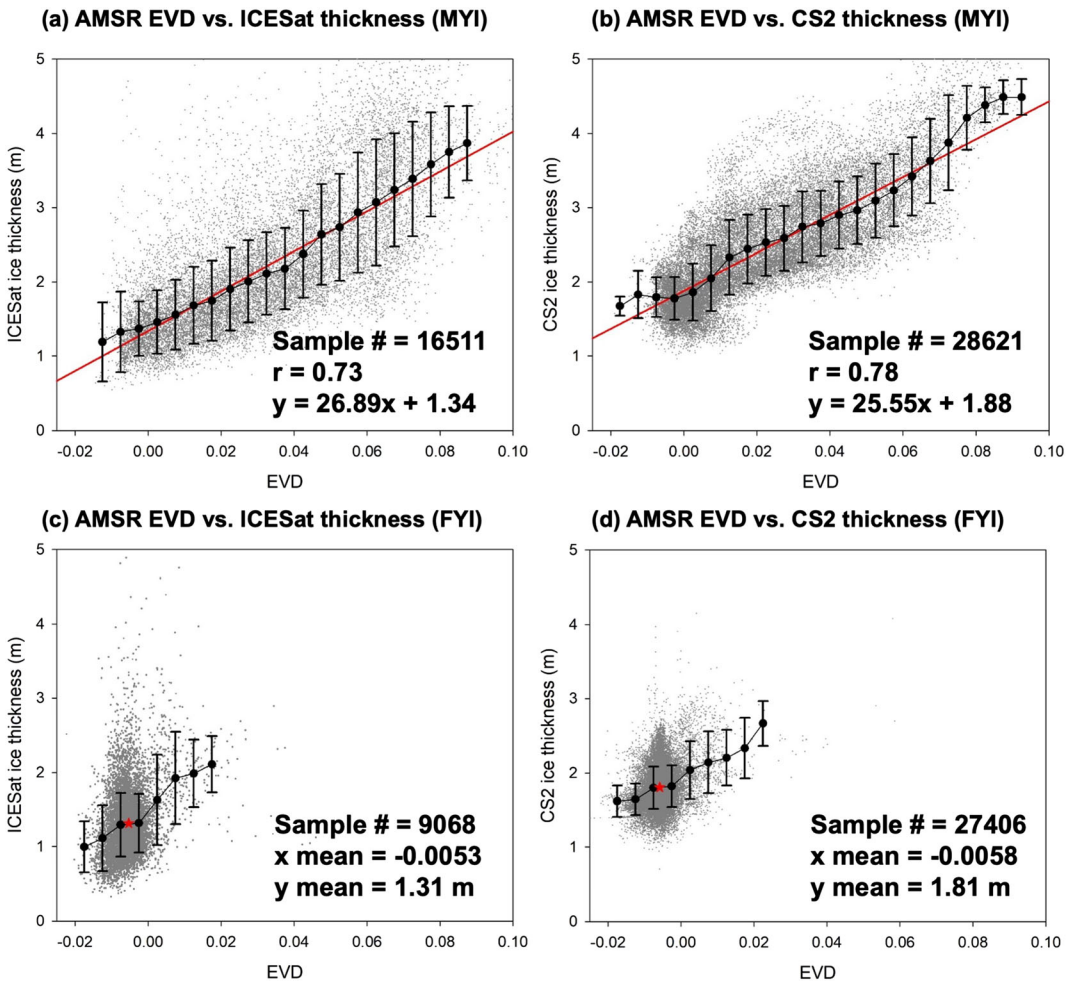

Figure 6. Scatterplots of (a) AMSR EVD versus ICESat thickness and (b) AMSR EVD versus CS2 thickness for multiyear sea ice (MYI). Red lines in the upper panels are linear regression lines, and one standard deviation is given with the mean for each binned EVD. Lower panels are for the first-year sea ice (FYI). Red dots in (c) and (d) show the sample means of EVD and ice thickness (x mean vs. y mean).

We interpreted the relative difference of 50 cm to be a systematic bias because the same EVD will likely yield a similar mean ice thickness over the 14 years of the analysis period. This is because the optical thickness should be largely controlled by the ice freeboard. It may be thought that the warming or snow depth change that occurred between the ICESat period (2004–2008) and CS2 period (2011–2018) also influenced the optical depth and thus contributed to the observed difference. However, considering that the freeboard will generally exhibit more scattering under the warming condition, due to more summer melting and brine drainage, the ice will become more porous and permeable (Perovich, 1996). Thus, the freeboard in March in the CS2 period will likely scatter more at 18.7 GHz, resulting in a larger EVD. Then, even for the same EVD values for ICESat and CS2 periods, the EVD in the latter CS2 period will have a *thinner* sea ice. Because of this reasoning, the expected warming-related impact, if there is any, should contribute in a direction opposite to the current ~50 cm thicker bias of CS2. Meanwhile, the possible impacts of variations in snow depth should be minor because the low-frequency microwave radiation is much less sensitive to such depths. Thus, the 50-cm bias can be counted as a systematic difference between the products of the two satellites.

As expected from the physical explanation, the first-year sea ice does not show a linear relationship between EVD and ice thickness. Instead, the plots of first-year ice show clusters of data points centered roughly at EVD = −0.0053 (thickness = 1.31 m) for ICESat and EVD = −0.0058 (thickness = 1.81 m) for CS2. The mean standard deviations from these mean thicknesses are 0.46 m for ICESat and 0.30 m for CS2. Even for the first-year sea ice, the CS2 ice thickness estimated later than ICESat is found to be thicker by ~50 cm, which is consistent with the 50 cm of bias noted between the two regression lines of multiyear sea ice.

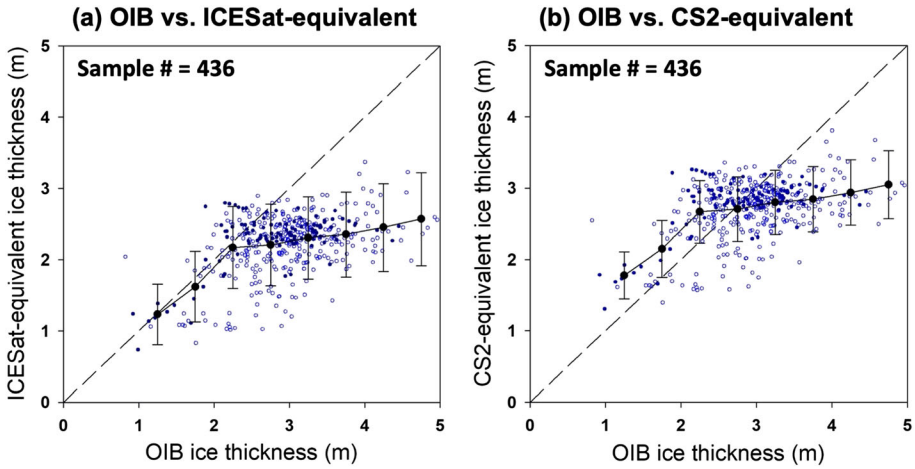

Figure 7. Scatterplot between OIB ice thickness versus (a) ICESat-equivalent ice thickness and versus (b) CS2-equivalent ice thickness. Filled and open blue dots represent OIB measurements on March and April, respectively. Vertical bar represents the error range of the estimated ice thickness for the binned OIB ice thickness, and black dot represents the mean ice thickness of the samples in each EVD bin.

4.1.2. Evaluation of Two Ice Thickness Estimates

In section 4.1.1, the sea ice thickness measured in the later period (i.e., CS2 data) was thicker, in spite of the expectation that Arctic sea ice has become thinner with time (Lindsay & Schweiger, 2015), although the direction of thinning should not be linear with time (or warming), as exemplified by the nearly constant sea ice extent in the 1990s (Winsor, 2001) or in the minimum sea ice extent in 2012 and following recovery (Swart et al., 2015). Therefore, one of the data sets is likely to be underestimated (or overestimated) respective to the other. However, assessing which data set has been underestimated or overestimated is difficult because a direct comparison is not permitted due to the 24-month gap between the two available data sets. To overcome this limitation, we apply the two regression equations delineated in Figure 6 to the common AMSR data to produce the ICESat- and CS2-equivalent sea ice thickness and then compare the obtained equivalent ice thickness against collocated OIB measurements to examine how the regression-estimated sea ice thickness differs from OIB measurements.

The regression used in this study was developed based on March data because March is the only month for which all four data sets (ICESat, CS2, AMSR, and OIB) are available. However, for the comparison against OIB data, April AMSR-E data are also included for validation because OIB data for March alone are insufficient for comparison. To construct the collocation data, instantaneous pixel-level, 40-m footprint OIB data were collocated for given observation dates (Table 2) using the same method as for the collocation of ICESat. Once AMSR-E brightness data were collocated, EVD was calculated from the AMSR-E 6.9 GHz-derived emission layer temperature and AMSR-E atmosphere-corrected brightness temperatures at 10.65 and 18.7 GHz. Both ICESat- and CS2-equivalent sea ice thicknesses were then calculated by applying their respective regression equations for comparison against collocated OIB observations. Although the regression equations were obtained for the multiyear sea ice, application is also made for the first-year sea ice because the regression equations go through the mean locations noted in the scatterplots (Figures 6c and 6d). The error ranges corresponding to binned EVD are simultaneously taken from the regression results shown in Figure 6 and the comparative results are shown in Figure 7. Notably, samples appear to be mostly multiyear sea ice because the OIB ice thickness is generally >2 m. This is because the OIB flight paths are concentrated over regions dominated by multiyear sea ice, such as the Central Arctic Ocean and Beaufort Sea (Kurtz et al., 2013).

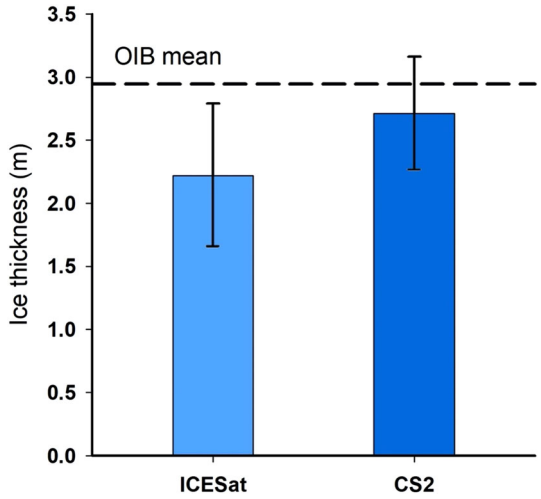

Figure 8. The mean and error range of ICESat-equivalent and CS2-equivalent ice thickness from 436 samples used for Figure 7 (colored bars). The mean OIB-estimated ice thickness is given as a dotted line, and error range is given at the top of each bar.

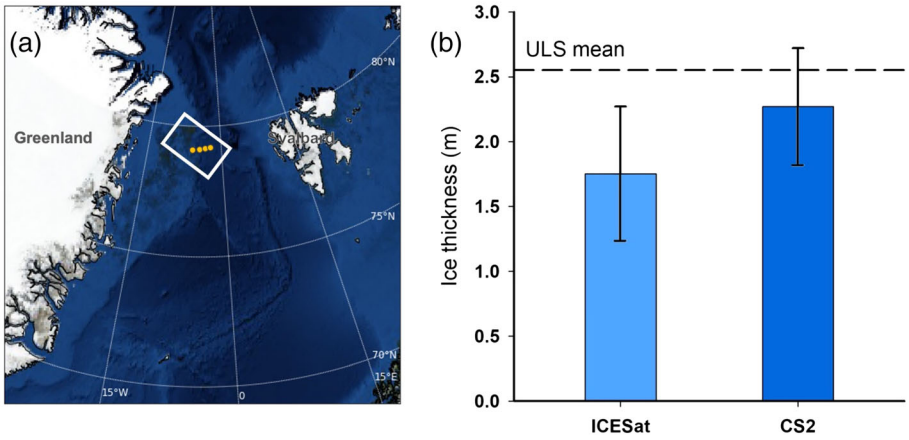

Figure 9. (a) Locations of ULS in Fram Strait (yellow dots)—adapted from Spreen et al. (2020). The white box surrounding the ULS locations is the area where satellite data are averaged and compared with ULS average. (b) The March mean and error range of ICESat-equivalent and CS2-equivalent ice thickness at the white grid box over the 2004–2014 period. Mean is given in vertical bar with error range at the top of each bar. The corresponding March mean ULS-derived ice thickness is given as a dotted line.

The results show that the CS2-equivalent ice thickness is in better agreement with the OIB ice thickness, as compared to the ICESat-equivalent ice thickness, which is most clearly seen in the mean value of the 436 samples used for comparison (Figure 8). The CS2-equivalent mean ice thickness of 2.71 m is closer to the OIB mean ice thickness of 2.95 m, when compared to the ICESat-equivalent mean ice thickness of 2.22 m. Taking the error ranges (±0.57 m for ICESat and ±0.45 m for CS2) into account, the mean OIB ice thickness is found to be within the error range for the CS2-equivalent, while it is outside of the error range for the ICESat-equivalent. Moreover, a mean bias of ~50 cm is clearly shown between the two altimeter-based equivalent ice thicknesses (Figure 8). The relative bias of ~50 cm suggests that there is an intrinsic difference between the two thickness data sets. The underestimate of ~50 cm by ICESat should be consistent with the mean bias of 50 cm for the first-year sea ice (compared with mean values of 1.31 vs. 1.81 m in Figures 6c and 6d). Considering that OIB measurements mostly cover regions with multi-year sea ice, nearly the same magnitude of the mean bias appears to exist regardless of ice age. One may concern about regression results based on multiyear ice only and then application to first-year ice as well. However, considering that regression equations based on the first-year and multi-year combined data also give similar ~50-cm bias, results obtained from the comparison with OIB data should be sound.

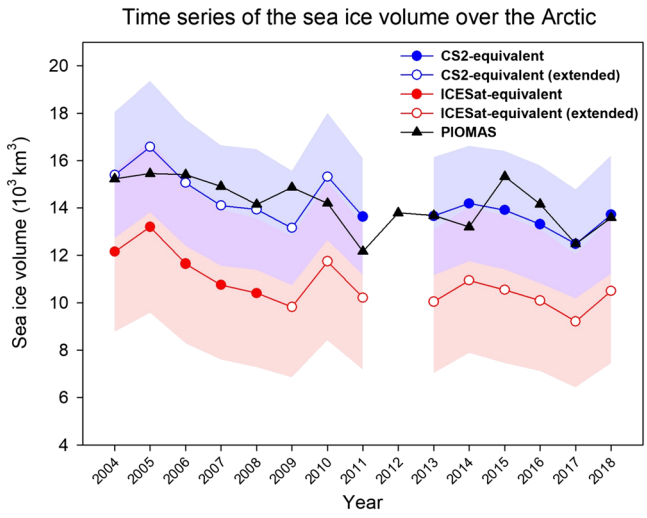

Figure 10. Time series of the sea ice volume from the ICESat-equivalent (red) and CS2-equivalent ice thickness (blue), along with the time series of the PIOMAS ice volume (black). Open dots in each colored line are results by applying the corresponding regression equation (obtained from the closed-dot observation period) to AMSR data. Error ranges caused by regression-based ice thickness errors are bounded by color shadings, and overlapped ranges are shaded with the pinkish-purple color.

Results obtained from comparison with OIB data should become more credible if similar results are found from other data at different region. Recently, Spreen et al. (2020) presented the time series of sea ice thickness from upward looking sonar (ULS) at the western part of Fram Strait. Although the sea ice thickness derived from point sea ice draft measurements from ULS may not be appropriate for the direct comparison with satellite retrievals, the comparison can shed light on whether the comparison results with OIB data are valid for other regions. Detailed explanation and data processing regarding the ULS data at Fram Strait are found in Spreen et al. (2020) and references therein. From the monthly mean time series of ice thickness during 1990–2014, presented in Figure 2 of Spreen et al. (2020), March mean ice thickness was obtained for the period of 2004–2014. On the other hand, ICESat- and CS2-equivalent ice thicknesses were calculated at the outlined box in Figure 9a by applying two regression equations to AMSR-derived EVDs for the overlapped 2004–2014 period, and they are called "ICESat-equivalent" and "CS2-equivalent," respectively. ICESat and CS2 averages and associated error

Table 3
Differential Forms of Equations 4 and 5 With Input Parameters

	$\frac{\partial h_i}{\partial x}$	
x : Input parameter	Equation 4 for lidar	Equation 5 for radar
h_{fs} : Snow depth (cm)	$-\frac{\rho_w-\rho_s}{\rho_w-\rho_i}$	$\frac{\rho_s}{\rho_w-\rho_i}$
ρ_i : Ice density (kg m^{-3})	$\frac{\rho_w(h_f-h_{fs})+\rho_s h_{fs}}{(\rho_w-\rho_i)^2}$	$\frac{\rho_w h_{fi}+\rho_s h_{fs}}{(\rho_w-\rho_i)^2}$
ρ_s : Snow density (kg m^{-3})	$\frac{h_{fs}}{\rho_w-\rho_i}$	$\frac{h_{fs}}{\rho_w-\rho_i}$
ρ_w : Seawater density (kg m^{-3})	$-\frac{\rho_i(h_f-h_{fs})+\rho_s h_{fs}}{(\rho_w-\rho_i)^2}$	$-\frac{\rho_i h_{fi}+\rho_s h_{fs}}{(\rho_w-\rho_i)^2}$

ranges were calculated for the comparison with ULS March mean over the 2004–2014 period. In this calculation, March of 2012 was excluded because of the AMSR data gap, and the area showing the sea ice concentration less than 95% was not counted because of the error caused by seawater in the microwave remote sensing.

Comparison results are given in Figure 9b. The 11-year March mean from ULS measurements in the western part of Fram Strait are found to be 2.52 m. The CS2-equivalent mean ice thickness of 2.27 m is closer to the ULS mean ice thickness of 2.52 m, when compared to the ICESat-equivalent mean ice thickness of 1.75 m. Taking the error ranges ($\pm$0.52 m for ICESat and $\pm$0.45 m for CS2) into account, the ULS mean ice thickness is found to be within the error range for the CS2-equivalent, while it is outside of the error range for the ICESat-equivalent. Thus, it suffices to conclude that results of the comparison with ULS measurements are consistent with results derived from the comparison with OIB measurements.

4.2. Interpretation of the Relative Bias and Trend Analysis

4.2.1. Impact of Snow Depth on the Data Difference

The relative bias noted in the scatterplot is likely due to the different sensitivities of lidar (ICESat) and radar (CS2) measurements to the snow depth, which are used as input for retrieval (Zygmuntowska et al., 2014). Owing to these differences, different hydrostatic balance equations involving snow depth must be used for lidar and radar altimetry (Kwok & Markus, 2018), as given below:

$$h_i = \left(\frac{\rho_w}{\rho_w-\rho_i}\right)h_f - \left(\frac{\rho_w-\rho_s}{\rho_w-\rho_i}\right)h_{fs}, \tag{4}$$

$$h_i = \left(\frac{\rho_w}{\rho_w-\rho_i}\right)h_{fi} + \left(\frac{\rho_s}{\rho_w-\rho_i}\right)h_{fs}, \tag{5}$$

where h_i is sea ice thickness, h_f and h_{fi} are the total and ice freeboards, h_{fs} is snow depth, and ρ_w, ρ_i, and ρ_s are the densities of seawater, sea ice, and snow, respectively. Thus, the sensitivity of the sea ice thickness to the uncertainty in snow depth, which can be expressed as a differentiation of the second term of the right-hand side in Equations 4 and 5 with the snow depth, should be quite different. The sensitivity was found to be approximately -7 for lidar and 3 for radar, suggesting that an error of $+5$ cm in snow depth can cause a bias of approximately -35 cm for ICESat but of $+15$ cm for CS2. Therefore, an uncertainty in snow depth of ~5 cm can cause a 50-cm relative bias, which is equivalent to the relative bias found in this study. This simple calculation demonstrates the way an error in snow depth may propagate into the resultant ice thickness, leading to the conclusion that the relative bias of ~50 cm between ICESat and CS2 values in Figure 6 may be due to uncertainties in the input snow depths.

In addition to the impact of uncertainties in snow depth, differences may also be attributed to uncertainties in other input parameters, such as the sea ice, snow, and seawater densities used in Equations 4 and 5. To examine the impacts of such parameters on the differences in the two data sets, differential forms of Equations 4 and 5 are introduced with each input parameter (Table 3). Each differential expression

Table 4
Calculated Sensitivities for Lidar- and Radar-Based Ice Thickness to Chosen Input Parameters and Their Associated Differences, Based Upon the Use of Input Values Given at the Bottom

$\frac{\partial h_i}{\partial x}$	$\frac{\partial h_i}{\partial x}$ at the reference state[a]		
	Equation 4 for lidar	Equation 5 for radar	Difference (radar-lidar)
$\frac{\partial h_i}{\partial h_{fs}}$ (m/cm)	−0.070	0.029	0.099
$\frac{\partial h_i}{\partial \rho_i}$ (m/kg m^{-3})	0.027	0.027	0.0
$\frac{\partial h_i}{\partial \rho_s}$ (m/kg m^{-3})	0.029	0.029	0.0
$\frac{\partial h_i}{\partial \rho_w}$ (m/kg m^{-3})	−0.025	−0.025	0.0

[a]h_f = 0.5 m, h_{fi} = 0.2 m, h_{fs} = 0.3 m, ρ_w = 1,024 kg m^{-3},ρ_i = 920 kg m^{-3}, and ρ_s = 300 kg m^{-3}.

represents the way in which the derived ice thickness is sensitive to a chosen input parameter. Approximate values of the sensitivity of the ice thickness to input parameters are then calculated using the input values of h_f = 0.5 m, h_{fi} = 0.2 m, h_{fs} = 0.3 m, ρ_w = 1,024 kg m^{-3}, ρ_i = 920 kg m^{-3}, and ρ_s = 300 kg m^{-3}. The obtained sensitivities (Table 4) show that the difference between data sets is not affected by any of those if the same value of any parameter is used in both radar and lidar equations. In contrast, the influence of snow depth on the difference is substantial, indicating that the snow depth is the main input parameter causing the differences between the two data sets, confirming the results of Zygmuntowska et al. (2014).

Other factors for the consideration of the different two ice thickness data may be different sea surface references employed by ICESat and CS2 missions and geophysical corrections such as wave propagation delay in the atmosphere and effects of various tides. For the freeboard measurement over the Arctic Ocean, ICESat uses the Arctic Gravity Project (ArcGP) geoid surface while CS2 uses Technical University of Demark (DTU) mean sea level data (Kurtz & Harbeck, 2017; Yi & Zwally, 2009). Skourup et al. (2017) examined the possible influence of different geoid references on freeboard measurement and reported that two different geoid references gave a near zero bias with a standard deviation of a few centimeters. The influences of different geophysical correction parameters on the freeboard appear to be negligible (Ricker et al., 2016). Thus, use of different reference surfaces and geophysical corrections should not be factors causing the bias of 50 cm noted in the study.

4.2.2. Trend Analysis

We examine how trends in ice volume during late winter (March) over the Arctic Ocean compared with the independent PIOMAS ice volume trend. For this purpose, the ICESat- and CS2-equivalent ice thicknesses are calculated by applying two regression equations to AMSR-derived EVDs for the period 2004–2018. As the two EVD-based regression equations exhibit a relative bias of ~50 cm, it is possible to examine how relative differences between the ICESat and CS2 ice thicknesses impact the estimates of changes in ice volume over the Arctic in comparison to the trend in volume against the independent, model-based PIOMAS volume trend. In this comparison, ice volumes are counted only over areas where the NSIDC sea ice concentration exceeds 95%.

The two trends in ice volume over time (ICESat- and CS2-equivalents) are shown together with the PIOMAS trend (Figure 10), along with the ranges of error induced by errors in the EVD-derived ice thickness. Because the EVD data from 2004 to 2008 and 2011 to 2018 were used to train their relationships to the ICESat and CS2 thicknesses, respectively, the trend connecting these two periods (between the red and blue solid dots in Figure 10) clearly shows that the volume sharply increased from the ICESat observation period (2004–2008) to that of CS2 (2011–2018). In fact, a similar abrupt increase in ice volume was observed when the observed ICESat (2004–2008) and CS2 (2011–2018) ice thicknesses were combined (not shown). Such a sharp increase seems improbable under the prevailing warming conditions and contrasts with the continuously decreasing trend observed in the PIOMAS data. However, when the regression equation for the CS2-equivalent ice thickness is applied to AMSR EVDs from 2004 to 2010, there is a

decreasing trend in ice volume quite similar to that suggested by PIOMAS. A similar trend is also found in the ICESat-equivalent ice thickness when calculations of ICESat-equivalent volume are extended beyond 2008 (i.e., 2009–2018). The similarity in the trends between ICESat and CS2 is obvious because the ice volume estimates are built with two linear equations, with signals derived from the AMSR measurements.

Kwok and Cunningham (2015) showed a decreasing trend in ice volume from the combination of ICESat and CS2 ice thickness data, in contrast to the suddenly increasing trend shown here; however, for the ICESat thickness data used in their study, European Centre for Medium-Range Weather Forecasts (ECMWF) snow depths were used, which differed from the snow data of Warren et al. (1999) used in this study for CS2 retrieval. In other words, because the sensitivity of the retrieved sea ice thickness to the input snow depth depends on the altimeter type, as shown in the sensitivity test, the use of different snow depth data (cf. Kwok & Cunningham, 2015) could explain the difference in sea ice thickness.

Even after considering the error ranges in the obtained ice volumes and trends, the EVD-based trend clearly shows that the ice volume decreases during the analysis period 2004–2018, which is consistent with the decreasing PIOMAS-derived trend. Since the backward extension of the CS2 regression equation to cover the ICESat period or the forward extension of the ICESat regression equation to cover the CS2 period should involve a simple adjustment for the relative bias of ~50 cm, it is believed that it is this adjustment that resulted in the decreasing trend. Thus, it is concluded that the relative bias of ~50 cm between ICESat and CS2 is also sound.

5. Conclusions

It is important to examine how two sets of satellite-borne, altimeter-based ice thickness data over the Arctic Ocean (ICESat and CS2) compare to one another because of the differences expected from measuring different parts of the freeboard and the different sensitivities of their retrieval algorithms to snow depth input. However, the gap in the observation period between ICESat and CS2 has hindered their direct comparison, which is essential for constructing a long-term data set from these two resources. In this study, the EVD—defined as the vertically polarized surface emissivity at 10.65 and 18.7 GHz—was used to estimate ice thickness by relating the EVD to the corresponding ice thickness; the EVD was then used as the shared platform for comparing the two data sets. The connection of the passive microwave EVD to the ice thickness is based on the different spectral nature of the optical properties of sea ice, which vary with the aging and thickening of the ice. When brines in the first-year sea ice are replaced by air pockets after surviving the summer, the resultant multiyear freeboard ice produces a deeper emission layer and more scattering by air pockets. Additionally, radiation emitted at a higher frequency (here, 18.7 GHz) is scattered more by the freeboard ice. Since the height of freeboard ice should be proportional to the total ice thickness, the EVD should contain information on ice thickness. Based on this physical reasoning, a linear relationship was drawn from the comparison of passive microwave EVDs with altimeter-based ice thickness. In contrast, due to the lesser scattering in first-year sea ice, no such relationship was found, enabling us to differentiate between the first-year and multiyear sea ice.

The EVD, which may be interpreted as an index of the difference in scattering between two channels (10.65 and 18.7 GHz) by the freeboard sea ice, varies mainly with changes in the optical properties of freeboard sea ice associated with its composition and height. Since the composition of sea ice freeboard should not have changed meaningfully with time during the 2004–2018 study period, the EVD may be used as a common platform over which two ice thickness data sets can be compared. In other words, the same EVD represents the similar mean signal for the freeboard sea ice (and thus ice thickness) throughout the combined ICESat and CS2 observation period. Based on this assumption, two ice thickness data sets were compared, and the results indicated the existence of a mean difference of ~50 cm between the ICESat and CS2 ice thickness data, regardless of ice type. The CS2-derived ice thickness appears to be larger than that of ICESat by 50 cm. Considering that the CS2 observation period was later than that of ICESat, such an increase in ice thickness is very unlikely to occur, given the well-established climatic warming over the Arctic. Validation of AMSR-derived ice thickness estimates against OIB measurements suggested that the 50-cm difference was more likely caused by an underestimation of sea ice thickness by ICESat rather than an overestimation by CS2, which appears to be largely caused by the different sensitivities of the two retrieval methods to errors in input snow depths.

The results of this study demonstrate that an adjustment for the relative difference of ~50 cm is needed to correct the ice thickness on either side of the observation period in order to accurately estimate trends in ice volume from the two non-overlapping data sets. With the adjusted data, the resultant decreasing trend in ice volume is consistent with that expected under the warming conditions. Furthermore, it is also consistent with the model-based PIOMAS trend when the adjustment is made, again confirming the existence of a systematic bias between the lidar-based ICESat and radar-based CS2 estimates of sea ice thickness.

Data Availability Statement

The data for producing figures are available on FigShare (https://doi.org/10.6084/m9.figshare.12904556).

Acknowledgments
The authors would like to thank the GCOM data center of JAXA for brightness temperatures and sea ice concentration data of AMSR-E and AMSR2 (https://gportal.jaxa.jp/gpr/search?tab=1), the NSIDC for sea ice thickness data of ICESat, CS2, OIB, and ice age data (http://nsidc.org/data/NSIDC-0393, https://nsidc.org/data/RDEFT4, http://nsidc.org/data/idcsi4/, and https://nsidc.org/data/nsidc-0611), and the PSC for PIOMAS model ice thickness data (http://psc.apl.uw.edu/research/projects/arctic-sea-ice-volume-anomaly/data/model_grid). This work was funded by the Space Core Technology Development Program (NRF-2018M1A3A3A02065661) and by the Korea Meteorological Administration Reasearch and Development Program under Grant KMIPA KMI2018-06910.

References

Cavalieri, D. J., Gloersen, P., & Campbell, W. J. (1984). Determination of sea ice parameters with the Nimbus 7 SMMR. *Journal of Geophysical Research*, *89*(D4), 5355–5369. https://doi.org/10.1029/JD089iD04p05355

Comiso, J. C. (1983). Sea ice effective microwave emissivities from satellite passive microwave and infrared observations. *Journal of Geophysical Research*, *88*(C12), 7686–7704. https://doi.org/10.1029/JC088iC12p07686

Comiso, J. C. (1995). *SSM/I sea ice concentrations using the bootstrap algorithm* (Vol. 1380). Greenbelt, MD: National Aeronautics and Space Administration, Goddard Space Flight Center.

Comiso, J. C., Cavalieri, D. J., & Markus, T. (2003). Sea ice concentration, ice temperature, and snow depth using AMSR-E data. *IEEE Transactions on Geoscience and Remote Sensing*, *41*(2), 243–252. https://doi.org/10.1109/TGRS.2002.808317

Cox, G. F., & Weeks, W. F. (1974). Salinity variations in sea ice. *Journal of Glaciology*, *13*(67), 109–120. https://doi.org/10.3189/S0022143000023418

Farrell, S. L., Kurtz, N., Connor, L. N., Elder, B. C., Leuschen, C., Markus, T., et al. (2011). A first assessment of IceBridge snow and ice thickness data over Arctic sea ice. *IEEE Transactions on Geoscience and Remote Sensing*, *50*(6), 2098–2111. https://doi.org/10.1109/TGRS.2011.2170843

Hewison, T. J., & English, S. J. (1999). Airborne retrievals of snow and ice surface emissivity at millimeter wavelengths. *IEEE Transactions on Geoscience and Remote Sensing*, *37*(4), 1871–1879. https://doi.org/10.1109/36.774700

Imaoka, K., Maeda, T., Kachi, M., Kasahara, M., Ito, N., & Nakagawa, K. (2012, November). Status of AMSR2 instrument on GCOM-W1. In *Earth observing missions and sensors: Development, implementation, and characterization II* (Vol. 8528, pp. 15-1–15-6). Bellingham, WA: International Society for Optics and Photonics. https://doi.org/10.1117/12.977774

Japan Aerospace Exploration Agency (JAXA) (2020). Intercomparison results between AMSR2 and TMI/AMSR-E/GMI (AMSR2 Version 2.0). [online] Suzaku.eorc.jaxa.jp. Retrieved from https://suzaku.eorc.jaxa.jp/GCOM_W/materials/product/150326_AMSR2_XcalResults.pdf, March 2015.

Kurtz, N., & Harbeck, J. (2017). *CryoSat-2 level-4 sea ice elevation, freeboard, and thickness, version 1*. Boulder, Colorado USA: NASA National Snow and Ice Data Center Distributed Active Archive Center. Retrieved From https://doi.org/10.5067/96JO0KIFDAS8 [Accessed 12 November 2020].

Kurtz, N. T., Farrell, S. L., Studinger, M., Galin, N., Harbeck, J. P., Lindsay, R., et al. (2013). Sea ice thickness, freeboard, and snow depth products from Operation IceBridge airborne data. *The Cryosphere*, *7*, 1035–1056. https://doi.org/10.5194/tc-7-1035-2013

Kurtz, N. T., Galin, N., & Studinger, M. (2014). An improved CryoSat-2 sea ice freeboard retrieval algorithm through the use of waveform fitting. *The Cryosphere*, *8*(4), 1217–1237. https://doi.org/10.5194/tc-8-1217-2014

Kwok, R., & Cunningham, G. F. (2008). ICESat over Arctic sea ice: Estimation of snow depth and ice thickness. *Journal of Geophysical Research*, *113*, C08010. https://doi.org/10.1029/2008JC004753

Kwok, R., & Cunningham, G. F. (2015). Variability of Arctic sea ice thickness and volume from CryoSat-2. *Philosophical Transactions of the Royal Society A: Mathematical, Physical and Engineering Sciences*, *373*, 20140157. https://doi.org/10.1098/rsta.2014.0157

Kwok, R., & Markus, T. (2018). Potential basin-scale estimates of Arctic snow depth with sea ice freeboards from CryoSat-2 and ICESat-2: An exploratory analysis. *Advances in Space Research*, *62*(6), 1243–1250. https://doi.org/10.1016/j.asr.2017.09.007

Lavergne, T., Sørensen, A. M., Kern, S., Tonboe, R., Notz, D., Aaboe, S., et al. (2019). Version 2 of the EUMETSAT OSI SAF and ESA CCI sea-ice concentration climate data records. *The Cryosphere*, *13*, 49–78. https://doi.org/10.5194/tc-13-49-2019

Laxon, S. W., Giles, K. A., Ridout, A. L., Wingham, D. J., Willatt, R., Cullen, R., et al. (2013). CryoSat-2 estimates of Arctic sea ice thickness and volume. *Geophysical Research Letters*, *40*, 732–737. https://doi.org/10.1002/grl.50193

Lee, S.-M., Sohn, B.-J., & Kim, S.-J. (2017). Differentiating between first-year and multiyear sea ice in the Arctic using microwave-retrieved ice emissivities. *Journal of Geophysical Research: Atmospheres*, *122*, 5097–5112. https://doi.org/10.1002/2016JD026275

Lee, S. M., Sohn, B.-J., & Shi, H. (2018). Impact of ice surface and volume scatterings on the microwave sea ice apparent emissivity. *Journal of Geophysical Research: Atmospheres*, *123*, 9220–9237. https://doi.org/10.1029/2018JD028688

Lindsay, R., & Schweiger, A. (2015). Arctic sea ice thickness loss determined using subsurface, aircraft, and satellite observations. *The Cryosphere*, *9*(1), 269–283. https://doi.org/10.5194/tc-9-269-2015

Markus, T., & Cavalieri, D. J. (2000). An enhancement of the NASA Team sea ice algorithm. *IEEE Transactions on Geoscience and Remote Sensing*, *38*(3), 1387–1398. https://doi.org/10.1109/36.843033

Mathew, N., Heygster, G., & Melsheimer, C. (2009). Surface emissivity of the Arctic sea ice at AMSR-E frequencies. *IEEE Transactions on Geoscience and Remote Sensing*, *47*(12), 4115–4124. https://doi.org/10.1109/TGRS.2009.2023667

Maykut, G. A. (1978). Energy exchange over young sea ice in the central Arctic. *Journal of Geophysical Research*, *83*(C7), 3646–3658. https://doi.org/10.1029/JC083iC07p03646

Maykut, G. A., & Untersteiner, N. (1971). Some results from a time-dependent thermodynamic model of sea ice. *Journal of Geophysical Research*, *76*(6), 1550–1575. https://doi.org/10.1029/JC076i006p01550

Meier, W. N., & Stewart, J. S. (2019). Assessing uncertainties in sea ice extent climate indicators. *Environmental Research Letters*, *14*, 035005. https://doi.org/10.1088/1748-9326/aaf52c

Peng, G., Matthews, J. L., & Yu, J. T. (2018). Sensitivity analysis of Arctic sea ice extent trends and statistical projections using satellite data. *Remote Sensing*, *10*(2), 230. https://doi.org/10.3390/rs10020230

Perovich, D. K. (1996). *The optical properties of sea ice* (pp. 1–24). Hanover, NH: US Army Corps of Eng. Cold Regions Research and Engineering Lab.

Ricker, R., Hendricks, S., & Beckers, J. F. (2016). The impact of geophysical corrections on sea-ice freeboard retrieved from satellite altimetry. *Remote Sensing*, *8*(4), 317. https://doi.org/10.3390/rs8040317

Schutz, B. E., Zwally, H. J., Shuman, C. A., Hancock, D., & DiMarzio, J. P. (2005). Overview of the ICESat mission. *Geophysical Research Letters*, *32*, L21S01. https://doi.org/10.1029/2005GL024009

Schweiger, A., Lindsay, R., Zhang, J., Steele, M., Stern, H., & Kwok, R. (2011). Uncertainty in modeled Arctic sea ice volume. *Journal of Geophysical Research*, *116*, C00D06. https://doi.org/10.1029/2011JC007084

Skourup, H., Farrell, S. L., Hendricks, S., Ricker, R., Armitage, T. W., Ridout, A., et al. (2017). An assessment of state-of-the-art mean sea surface and geoid models of the Arctic Ocean: Implications for sea ice freeboard retrieval. *Journal of Geophysical Research: Oceans*, *122*, 8593–8613. https://doi.org/10.1002/2017JC013176

Spreen, G., de Steur, L., Divine, D., Gerland, S., Hansen, E., & Kwok, R. (2020). Arctic sea ice volume export through Fram Strait from 1992 to 2014. *Journal of Geophysical Research: Oceans*, *125*, e2019JC016039. https://doi.org/10.1029/2019JC016039

Spreen, G., Kaleschke, L., & Heygster, G. (2008). Sea ice remote sensing using AMSR-E 89-GHz channels. *Journal of Geophysical Research*, *113*, C02S03. https://doi.org/10.1029/2005JC003384

Stroeve, J., Blanchard-Wrigglesworth, E., Guemas, V., Howell, S., Massonnet, F., & Tietsche, S. (2015). Improving predictions of Arctic sea ice extent. *Earth and Space Science*, *96*, 11. https://doi.org/10.1029/2015EO031431

Swart, N. C., Fyfe, J. C., Hawkins, E., Kay, J. E., & Jahn, A. (2015). Influence of internal variability on Arctic sea-ice trends. *Nature Climate Change*, *5*(2), 86. https://doi.org/10.1038/nclimate2483

Tonboe, R. T., Eastwood, S., Lavergne, T., Sørensen, A. M., Rathmann, N., Dybkjær, G., et al. (2016). The EUMETSAT sea ice concentration climate data record. *The Cryosphere*, *10*, 2275–2290. https://doi.org/10.5194/tc-10-2275-2016

Tschudi, M., Meier, W. N., Stewart, J. S., Fowler, C., & Maslanik, J. (2019). EASE-Grid Sea Ice Age, Version 4 | National Snow And Ice Data Center. Retrieved from https://doi.org/10.5067/UTAV7490FEPB [Accessed 12 November 2020].

Warren, S. G., Rigor, I. G., & Untersteiner, N. (1999). Snow depth on Arctic sea ice. *Journal of Climate*, *12*, 1814–1825. https://doi.org/10.1175/1520-0442(1999)012<1814:SDOASI>2.0.CO;2

Wingham, D. J., Francis, C. R., Baker, S., Bouzinac, C., Brockley, D., Cullen, R., et al. (2006). CryoSat: A mission to determine the fluctuations in Earth's land and marine ice fields. *Advances in Space Research*, *37*(4), 841–871. https://doi.org/10.1016/j.asr.2005.07.027

Winsor, P. (2001). Arctic sea ice thickness remained constant during the 1990s. *Geophysical Research Letters*, *28*(6), 1039–1041. https://doi.org/10.1029/2000GL012308

World Meteorological Organization (WMO). (2020). WMO OSCAR | Satellite: Cryosat-2. [online] Wmo-sat.info. Retrieved from http://www.wmo-sat.info/oscar/satellites/view/39 [Accessed 12 November 2020].

Yi, D., & Zwally, H. J. (2009). Arctic Sea Ice Freeboard And Thickness, Version 1 | National Snow And Ice Data Center. Retrieved from https://doi.org/10.5067/SXJVJ3A2XIZT [Accessed 12 November 2020].

Yi, D., Zwally, H. J., & Robbins, J. W. (2011). ICESat observations of seasonal and interannual variations of sea-ice freeboard and estimated thickness in the Weddell Sea, Antarctica (2003–2009). *Annals of Glaciology*, *52*(57), 43–51. https://doi.org/10.3189/172756411795931480

Zwally, H. J., Schutz, B., Abdalati, W., Abshire, J., Bentley, C., Brenner, A., et al. (2002). ICESat's laser measurements of polar ice, atmosphere, ocean, and land. *Journal of Geodynamics*, *34*(3–4), 405–445. https://doi.org/10.1016/S0264-3707(02)00042-X

Zygmuntowska, M., Rampal, P., Ivanova, N., & Smedsrud, L. H. (2014). Uncertainties in Arctic sea ice thickness and volume: New estimates and implications for trends. *The Cryosphere*, *8*(2), 705–720. https://doi.org/10.5194/tc-8-705-2014